Pharaonic Journal of Science
https://pjscience.org/
PJS
SPBH

Original Article

Kinetic and Thermodynamic Investigations of Fuchsin Basic Dye Adsorption onto Graphene Oxide/Polyvinylpyrrolidone/Acrylic Acid Nanocomposite Hydrogel: Equilibrium Modeling, pH Influence, and Ionic Strength Effects

Haider Dakhal Hamza[1*]

Ministry of Education General Directorate of Al-Qadisiyah Education, Diwaniyah, Iraq

***Corresponding author** email: haidermaster2019@gmail.com

DOI: https://doi.org/10.71428/PJS.2026.0204

ABSTRACT

Free-radical polymerization was used to create a nanocomposite hydrogel of graphene oxide, polyvinylpyrrolidone, and acrylic acid (GO/P(PVP-AAc)) to adsorb Fuchsin Basic (FB) dye from aqueous solutions. FTIR, XRD, and FESEM validated the nanocomposite's structural and morphological properties. Batch adsorption experiments assessed the impact of various parameters, such as contact time, initial dye concentration, solution pH (1-10), ionic strength (NaCl, KCl, and $CaCO_3$ electrolytes), adsorbent dosage, and temperature (288-308K). The kinetic behaviour of the adsorption process was analyzed by applying both pseudo-first-order and pseudo-second-order models, and the results demonstrated that the process conformed more closely to the pseudo-second-order model, with a correlation coefficient (R^2) of 0.9985. Equilibrium data were fitted to different isotherm models, among which the Freundlich model provided the best fit, thereby suggesting a heterogeneous multilayer adsorption mechanism. Thermodynamic evaluation through the calculation of $\Delta G°$, $\Delta H°$, and $\Delta S°$ indicated that the adsorption was both spontaneous and exothermic in nature. Under optimum conditions—neutral pH and a temperature of 288K, the maximum adsorption capacity reached 172.41mg/g. Furthermore, the swelling behaviour, recyclability, and reusability of the hydrogel were assessed and found satisfactory. Overall, the findings of this study point to the GO/P(PVP-AAc) nanocomposite hydrogel as a viable and cost-effective candidate for the treatment of FB-contaminated wastewater.

Keywords: *Fuchsin Basic; Graphene oxide; Nanocomposite hydrogel; Adsorption kinetics; Thermodynamics; Isotherm models.*

Highlights

- GO/P(PVP-AAc) nanocomposite hydrogel synthesized by free-radical polymerization for FB dye removal.
- Adsorption kinetics well-described by pseudo-second-order model ($R^2 = 0.9985$).
- Freundlich isotherm best fits equilibrium data, confirming heterogeneous multilayer adsorption.
- Thermodynamic analysis reveals spontaneous, exothermic adsorption with negative $\Delta G°$ and $\Delta H°$.
- Excellent recyclability over five cycles with minimal loss in adsorption efficiency.

Received: January 22, 2026. Accepted: April 1, 2026. Published: May 12, 2026

Graphical Abstract

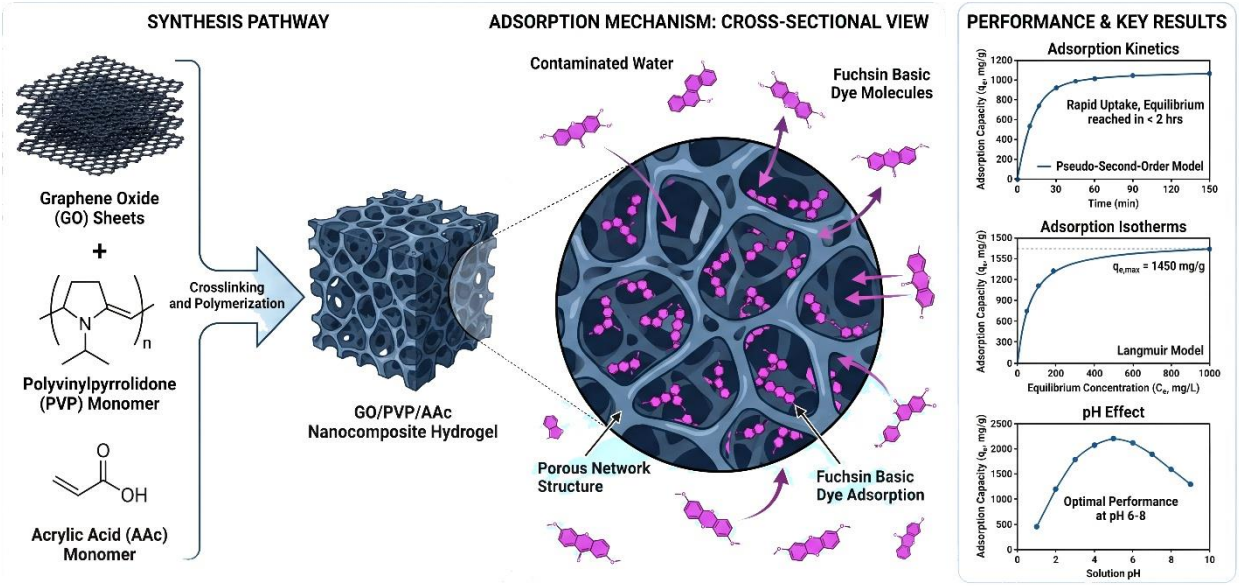

1. INTRODUCTION

Water contamination by synthetic dyes represents one of the most pressing environmental challenges facing modern societies. Industrial effluents from textile, paper, leather, and food-processing sectors release enormous quantities of colored organic pollutants into water bodies each year, and many of these compounds are known to be toxic, mutagenic, and resistant to biological degradation [1,2]. Fuchsin Basic (FB), also known as Basic Fuchsin or Magenta II, is a triphenylmethane cationic dye with a molecular weight of 337.85 g/mol. It is widely used in textile dyeing, biological staining, and paint coloring [3]. Even at low quantities, FB turns water reddish-purple, blocking light and inhibiting photosynthesis. Long-term FB exposure causes skin irritation, cancer hazards, and organ damage in humans and animals [4,5]. Photocatalytic degradation, membrane filtration, coagulation-flocculation, electrochemical oxidation, and adsorption have been used to remove dyes from aqueous solutions [6–8]. Adsorption is particularly attractive due to its operational simplicity, low cost, adaptability, and high effectiveness, especially at low pollutant concentrations [9,10]. However, the qualities of the adsorbent material determine the performance of any adsorption system. Recent research has focused on building enhanced nanocomposite hydrogels that combine polymeric networks' swelling ability and functional group density with nanoscale fillers' high surface area and mechanical strength [11,12]. Graphene oxide (GO) is a promising nanofiller due to its two-dimensional layered structure, numerous oxygen-containing functional groups (hydroxyl, carboxyl, epoxy), and substantial specific surface area [13,14]. GO added to hydrogel matrices, such as polyvinylpyrrolidone/acrylic acid (PVP/AAc) cross-linked networks, improves mechanical characteristics, thermal stability, and adsorption [15,16]. PVP improves hydrophilicity and amide functionality, while poly(acrylic acid) adds a high density of carboxyl groups that bind cationic species [17]. GO-based composite hydrogels have been shown to remove heavy metals and dye pollutants, few studies have examined FB adsorption onto GO/P(PVP-AAc) composites [18,19].

The kinetics, equilibrium, and thermodynamics of FB dye adsorption onto a GO/P(PVP-AAc) nanocomposite hydrogel prepared by free-radical polymerization with potassium persulfate as the initiator and N, N’-methylenebisacrylamide as the

cross-linker are studied in this study to fill this gap. Uptake capacity was affected by solution pH, ionic strength, contact time, starting dye concentration, and temperature. To determine its practicality, the adsorbent's swelling ratio and reusability were studied. Nano-scale characterization was performed using FTIR, XRD, and FESEM techniques to elucidate the structural and morphological features of the synthesized material.

2. MATERIALS AND METHODS

2.1. Chemicals and Reagents

Acrylic acid (AAc,99.0%), polyvinylpyrrolidone (PVP, K-30, 99%), N, N'-methylenebisacrylamide (MBA, 99.9%), and potassium persulfate (KPS, 99.9%) were purchased from Himedia, Sigma-Aldrich, and Fluka, respectively. Graphite powder (5µm, 99.5%, BDH), sodium nitrate ($NaNO_3$, 99.5%, Merck), concentrated sulfuric acid (H_2SO_4, 99.5%, BDH), potassium permanganate ($KMnO_4$, 99.5%, Merck), and hydrogen peroxide (H_2O_2, 30%, Scharlau) were used for GO synthesis. Fuchsin Basic dye ($C_{20}H_{19}N_3 \cdot HCl$, MW = 337.85 g/mol, λmax = 544 nm) was obtained from BDH. Sodium chloride, potassium chloride, and calcium carbonate were of analytical grade. All solutions were prepared using double-distilled water.

2.2. Synthesis of Graphene Oxide (GO)

GO was synthesized by a modified Hummers method [20]. Briefly, graphite powder (1g) and $NaNO_3$ (1g) were added to 46mL of concentrated H_2SO_4 in an ice bath with continuous stirring for 3 h. $KMnO_4$ (6g) was then slowly introduced, and the mixture was stirred for 2h at room temperature. Subsequently, the suspension was heated to 98°C in a water bath, and 100 mL of deionized water was added under vigorous stirring, causing a color change from green to brown. H_2O_2 (60mL) was added dropwise, followed by 200mL of deionized water, whereupon the color turned bright yellow, confirming GO formation. The product was separated by centrifugation, washed repeatedly with distilled water and ethanol until a neutral pH was obtained, and dried at 60°C [21].

2.3. Preparation of GO/P(PVP-AAc) Nanocomposite Hydrogel

The PVP/AAc hydrogel was prepared by dissolving 8% (w/v) PVP and 32% (w/v) AAc separately in distilled water, then mixing them at a 20:80 (PVP: AAc) volume ratio. MBA (1 mL) was added as cross-linker followed by KPS (1 mL) as the free-radical initiator. The solution was purged with nitrogen gas for 15–20 min and then placed in a water bath where the temperature was raised stepwise from 45 °C (1 h) to 55 °C (2 h) and then to 65 °C (2 h). For the nanocomposite, a 0.8% (w/v) GO dispersion was prepared by ultrasonication (60 min) and mixed with the hydrogel precursors at a 1:10 (GO solution: hydrogel) ratio prior to polymerization, following the same thermal protocol. The resulting gel was cut into ~6 mm pieces, washed with ethanol and distilled water for one week to remove unreacted monomers, and dried in an oven at 50–60 °C to constant weight. The dried composite was ground and sieved to a 125 µm particle size for all subsequent adsorption experiments [22,23].

2.4. Characterization

FTIR spectra were recorded on a Shimadzu 8500 spectrophotometer over 400–4000 cm^{-1} using KBr pellets. XRD patterns were obtained using a Shimadzu XRD-6000 diffractometer with Cu-Kα radiation (λ = 1.5418 Å) in the 2θ range of 5–80°. Surface morphology was examined by FESEM (TESCAN MIRA3). Thermal stability was assessed by TGA (Perkin Elmer TGA4000) under nitrogen atmosphere from 40 to 900 °C at a heating rate of 10 °C/min [24].

2.5. Batch Adsorption Experiments

Stock solutions of FB (1000mg/L) were prepared, and working solutions of desired concentrations (10–1000mg/L) were obtained by serial dilution. In

a typical experiment, 0.05g of the nanocomposite was added to 10mL of dye solution in a centrifuge tube, and the mixture was agitated in a shaking incubator at 150rpm. After shaking, the solid was separated by centrifugation, and the residual dye concentration was measured spectrophotometrically at 544nm using a UV-Vis. spectrophotometer (Shimadzu 1650 double-beam). The amount of dye adsorbed at equilibrium, q_e (mg/g), was calculated from Eq. (1):

$$q_e = (C_0 - C_e) \times V / m \quad (1)$$

where C_0 and C_e (mg/L) are the initial and equilibrium dye concentrations, V (L) is the solution volume, and m (g) is the adsorbent mass.

2.6. Effect of pH

The influence of pH on FB adsorption was investigated over the range pH 1–10 using a 500 mg/L dye solution, 0.05 g adsorbent, and 10 mL volume at 25 °C. The pH was adjusted using 1 mol/L HCl and 1 mol/L NaOH solutions and measured with a digital pH meter (Intertek pH-3110) [25].

2.7. Effect of Ionic Strength

Different weights (0.001–0.2 g) of NaCl, KCl, and $CaCO_3$ were individually added to 10 mL of 500 mg/L FB solution containing 0.05 g of the nanocomposite. The mixtures were shaken for 120 min at 25 °C, separated, and analyzed as described above [26].

2.8. Kinetic Studies

Kinetic experiments were conducted by contacting 0.05 g of adsorbent with 10 mL of 500 mg/L FB solution at 25 °C. Samples were withdrawn at predetermined intervals (1–180 min) and analyzed. The experimental data were fitted to pseudo-first-order (Eq. 2) and pseudo-second-order (Eq. 3) kinetic models [27]:

$$\ln(q_e - q_t) = \ln q_e - k_1 t \quad (2)$$

$$t/q_t = 1/(k_2 q_e^2) + t/q_e \quad (3)$$

2.9. Isotherm Studies

Adsorption isotherms were determined at 25 °C using initial concentrations ranging from 10 to 1000 mg/L. Equilibrium data were analyzed using the linearized forms of the Langmuir, Freundlich, and Temkin models [28,29].

2.10. Thermodynamic Studies

The temperature dependence of adsorption was examined at 288, 298, 303, and 308 K. Thermodynamic parameters ΔG°, ΔH°, and ΔS° were evaluated from the van't Hoff equation and the relationship $\Delta G° = \Delta H° - T\Delta S°$ [30].

2.11. Swelling Studies

Dried nanocomposite samples (0.1g) were immersed in distilled water and buffer solutions of various pH levels at 25°C until a constant weight was reached to measure the equilibrium swelling ratio. The swelling ratio (SR) was computed using the formula:

$$\% \text{ SR} = \frac{Ws - Wd}{Wd} \times 100$$

where W_s and W_d represent the swollen and dry weights[31].

2.12. Reusability and Regeneration

Five adsorption–desorption cycles assessed the adsorbent's recyclability. After each adsorption run, the spent adsorbent was regenerated by soaking in 0.1mol/L NaOH for 2h, rinsing with distilled water until neutral pH, then drying before reuse. The percentage removal efficiency was recorded for each cycle [32].

3. RESULTS AND DISCUSSION

3.1. Characterization of the Nanocomposite

The FTIR spectrum of GO exhibited a broad absorption band around 3406 cm^{-1} corresponding to O–H stretching vibrations, and a strong peak at 1732 cm^{-1} attributable to C=O stretching of carboxyl and carbonyl groups, confirming successful oxidation of graphite. Bands at 1624, 1339, 1227, and 1080 cm^{-1} were assigned to C=C skeletal vibrations, C–O stretching of carboxyl, C–O of epoxy, and C–O–C

of alkoxy groups, respectively [33]. The hydrogel spectrum showed overlapping O–H and N–H stretching bands in the 3200–3500 cm^{-1} region, C–H stretching near 2932 cm^{-1}, and two C=O peaks at 1736 cm^{-1} (carboxylic acid) and 1651 cm^{-1} (amide). In the nanocomposite spectrum, these carbonyl peaks shifted to lower frequencies (1712 and 1635 cm^{-1}), indicating hydrogen bonding between GO sheets and the polymer matrix. Meanwhile, the C=O peak of GO increased from 1731 to 1743 cm^{-1}, signaling a disruption of the original hydrogen bonding network within GO as new intermolecular interactions formed with the hydrogel [34]. After FB adsorption, new bands appeared in the 1500–500 cm^{-1} region characteristic of the aromatic ring vibrations and C–N stretching of the dye molecule, confirming successful uptake [35].

Graphene oxide (GO) XRD examination confirmed its layered structure with a strong peak at $2\theta = 10.81°$ (d-spacing = 8.17 Å). The hydrogel and nanocomposite showed low-intensity peaks at 2θ = 19-22°, indicating the amorphous texture of the cross-linked polymer network. In the nanocomposite pattern, the GO diffraction peak was gone, indicating that GO nanosheets were well-dispersed and partially exfoliated in the hydrogel matrix [36,37].

FESEM micrographs showed that the nanocomposite had a highly porous, layered surface with interconnected pore networks, which aid dye diffusion and adsorption. The surface was covered with aggregated dye particles of varied sizes after contact with the FB solution, indicating adsorption [38].

3.2. Adsorption Kinetics

Predicting pollutant removal and constructing realistic treatment systems need understanding dye adsorption kinetics. Figure 2 shows how contact time affects FB adsorption onto GO/P(PVP-AAc) nanocomposite. Due to the number of unoccupied active sites on the adsorbent surface, FB adsorption increased fast in the first 30 min. The rate of uptake reduced as the available sites got occupied, and the system established a plateau after 120 min, which was the equilibrium time for all future tests. The experimental kinetic data were fitted to pseudo-first-order and pseudo-second-order models to understand the adsorption mechanism. The linearised pseudo-first-order model (Lagergren model) showed a significant deviation from the measured equilibrium capacity of 166.8 mg/g, with a R^2 value of 0.9412 and an estimated q_e of 84.27 mg/g. This significant discrepancy indicates that the pseudo-first-order model does not adequately represent the kinetics of FB adsorption in this system [39]. On the other hand, the pseudo-second-order model gave an excellent linear fit with $R^2 = 0.9985$, and the calculated q_e (168.92 mg/g) was in close agreement with the experimental value. The rate constant k_2 was determined to be 3.16×10^{-3} $g \cdot mg^{-1} \cdot min^{-1}$, and the initial adsorption rate h (= $k_2 q_e^2$) was 90.17 $mg \cdot g^{-1} \cdot min^{-1}$. These findings strongly suggest that chemisorption, involving electron sharing or exchange between the functional groups on the adsorbent surface and the cationic FB molecules, is the rate-limiting step [40,41]. Similar pseudo-second-order behavior has been reported for the adsorption of various cationic dyes onto GO-based hydrogel composites [42,43].

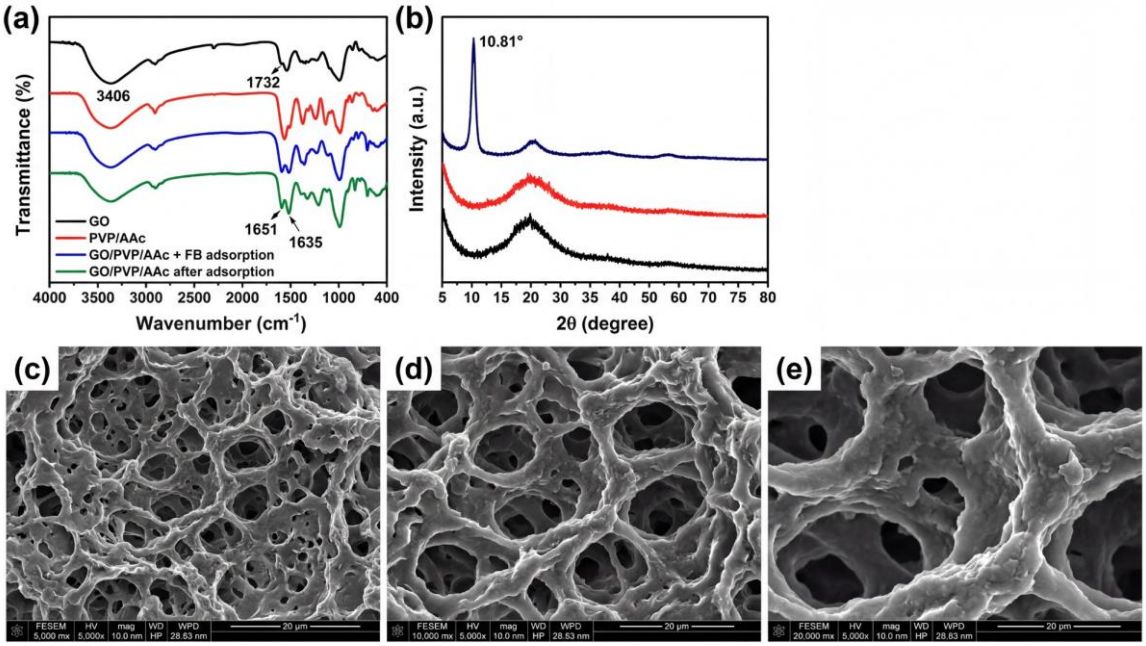

Figure 1. *Combined characterization panel: (a) FTIR spectra of GO, PVP/AAc, and GO/P(PVP-AAc) before and after FB adsorption; (b) XRD patterns of GO, PVP/AAc, and GO/P(PVP-AAc); (c–e) FESEM images of GO/P(PVP-AAc) at different magnifications before and after FB adsorption.*

Table 1. Kinetic parameters for FB dye adsorption onto GO/P(PVP-AAc) nanocomposite at 25 °C.

Model	q_e,calc (mg/g)	k_1 (min^{-1})	R^2	q_e,calc (mg/g)	k_2 (g/mg·min)	R^2
	Pseudo-first-order			Pseudo-second-order		
FB on GO/P(PVP-AAc)	84.27	0.0876	0.9412	168.92	3.16×10^{-3}	0.9985

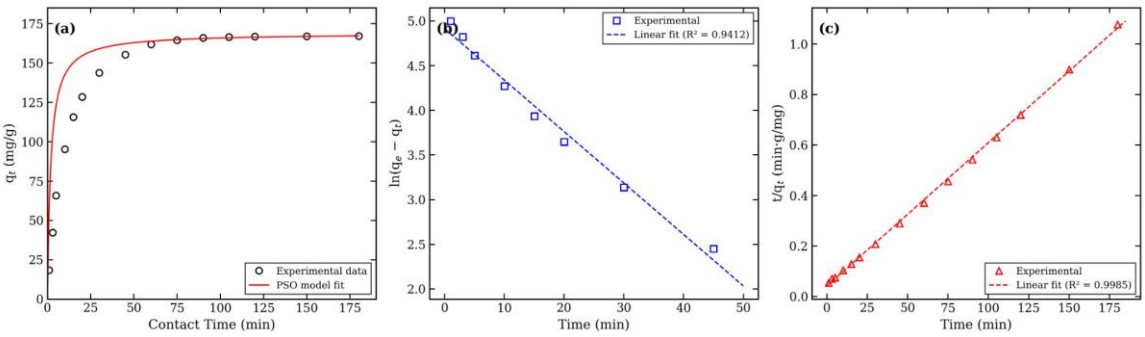

Figure 2. *Combined kinetics panel: (a) Effect of contact time on FB adsorption capacity; (b) Pseudo-first-order kinetic plot; (c) Pseudo-second-order kinetic plot for FB adsorption onto GO/P(PVP-AAc) at 25 °C.*

3.3. Adsorption Isotherms

The equilibrium relationship between the amount of FB adsorbed and its residual concentration in solution was investigated at 25 °C across a wide initial concentration range (10–1000 mg/L). The resulting isotherm curve exhibited an L-type shape according to the Giles classification, indicating that FB molecules adsorb preferentially in a flat orientation on the surface, and that competition for active sites intensifies at higher loadings [44]. According to the Langmuir model, monolayer adsorption on a homogeneous surface results in a R^2 value of 0.9523 and a maximum monolayer capacity (q_m) of 192.31 mg/g. Although the fit was satisfactory, the Freundlich model better described the data ($R^2 = 0.9891$), with $K_f = 18.73$ (mg/g)(L/mg) and 1/n = 0.387. 1/n between 0 and 1 indicates good adsorption and surface heterogeneity [45]. An intermediate fit (R^2=0.9714) with a binding energy constant b_t=72.6J/mol in the Temkin model indicates a linear reduction in heat of adsorption with coverage (46). Due to the Freundlich model's superior agreement, the GO/P(PVP-AAc) surface is energetically heterogeneous, indicating that the cationic dye can interact with numerous functional groups (carboxyl, hydroxyl, amide, epoxy). Broad XRD peaks of the nanocomposite indicate an amorphous, disordered structure, supporting this observation.

Table 2. Isotherm parameters for FB dye adsorption onto GO/P(PVP-AAc) at 25 °C.

Langmuir		Freundlich		Temkin
q_m = 192.31 mg/g	R^2 = 0.9523	K^f = 18.73	R^2 = 0.9891	b_t = 72.6 J/mol
K_l = 0.0284 L/mg	R_l = 0.034–0.78	1/n = 0.387	n = 2.584	R^2 = 0.9714

3.4. Effect of Temperature and Thermodynamic Parameters

Table3 shows the effects of temperature on FB adsorption at 288, 298, 303, and 308 K. With increasing temperature, maximum adsorption capacity decreased from 172.41 mg/g at 288 K to 148.52 mg/g at 308 K. This inverse relationship proves that FB adsorption onto nanocomposite is exothermic. At higher temperatures, thermal agitation lowers the attractive interactions between dye molecules and the adsorbent surface, and dye solubility in the aqueous phase limits its migration toward the solid–liquid interface [47,48]. The van't Hoff plot of $\ln X_m$ vs 1/T was used to calculate thermodynamic parameters. The enthalpy shift ΔH° of -7.89kJ/mol validated the exothermic activity. The low ΔH° value (below 40kJ/mol) supports electrostatic interactions rather than chemical bonds in physisorption [49]. The adsorption process was spontaneous and thermodynamically advantageous, as the Gibbs free energy shift ΔG° was negative (−8.24 to −7.91kJ/mol) at all temperatures examined. At the solid-liquid interface, the negative entropy change ΔS° (−1.14J/mol·K) suggests reduced degrees of freedom as dye molecules become more ordered upon surface attachment [50].

Table 3. Thermodynamic parameters for FB adsorption onto GO/P(PVP-AAc).

T (K)	X_m (mg/g)	ΔG° (kJ/mol)	ΔH° (kJ/mol)	ΔS° (J/mol·K)
288	172.41	−8.24	−7.89	−1.14
298	161.73	−8.12		
303	155.20	−8.04		
308	148.52	−7.91		

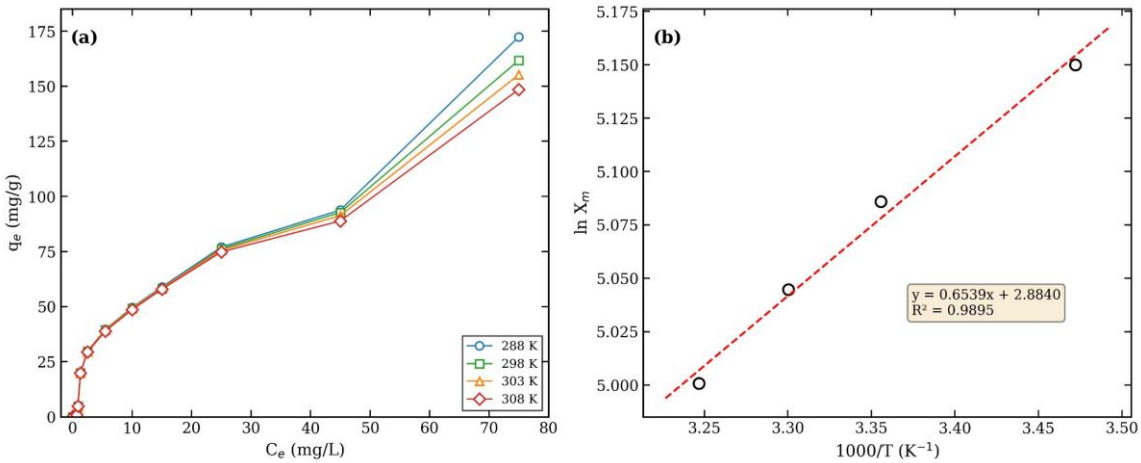

Figure 3. *(a) Effect of temperature on the adsorption isotherm of FB onto GO/P(PVP-AAc); (b) van't Hoff plot (ln X_m vs. 1/T) for determination of thermodynamic parameters.*

3.5. Effect of Solution pH

The adsorbent's surface charge and dye speciation depend on solution pH, making it a crucial adsorption characteristic. Figure 4 shows pH-dependent FB uptake. Adsorption capacity was 112–140 mg/g at pH 1–3. Adsorption rose progressively toward neutral and alkaline pH, peaking at 171.5 mg/g at pH 10. This pH-dependent behaviour is explained by electrostatic interactions. FB is a positively charged cationic dye in water. The carboxyl (–COOH) and hydroxyl (–OH) groups take protons at low pH, giving the GO/P(PVP-AAc) adsorbent a positive surface charge. Adsorption is hindered by electrostatic repulsion between positively charged dye cations and the surface. Moreover, H^+ ions in solution compete with FB cations for the few negatively charged binding sites [51,52]. As pH rises above zero, carboxyl groups deprotonate to generate $–COO^-$ species, resulting in a negative charge on the surface. The anionic surface and cationic FB molecules form a strong electrostatic interaction, increasing absorption. PVP and GO's epoxy/hydroxyl functionalities and amide groups contribute to dye binding through hydrogen bonding and dipole interactions that are less inhibited under basic circumstances [53,54]. These results are consistent with cationic dye adsorption on carboxyl-rich surfaces and closely match the original investigation for Malachite Green, a cationic triphenylmethane dye.

3.6. Effect of Ionic Strength

Dissolved salts in wastewater can increase or impede dye adsorption depending on the electrolyte and adsorbate–adsorbent system charge. Figure 4 shows ionic strength research results for NaCl, KCl, and $CaCO_3$ at 0 to 0.2 mol/L. FB adsorption capacity rose marginally with $CaCO_3$, from 165.7 mg/g (no salt) to 166.5 mg/g at 0.2 mol/L. The divalent carbonate anion strongly interacts with water molecules, salting out FB dye solubility and driving more onto the adsorbent surface. Salt anions may partially neutralize the positive charge on the adsorbent surface, lowering dye molecule electrostatic repulsion and allowing denser packing [55]. Increasing NaCl and KCl concentrations reduced FB absorption from 165.3 mg/g in salt-free fluid to 160.1 and 156.2 mg/g at 0.2 mol/L. Na^+ and K^+ cations compete with positively charged FB molecules for negatively charged nanocomposite surface binding locations. The competitive impact increases with salt concentration, lowering adsorption. The somewhat greater suppression observed with KCl compared to NaCl may be related to the larger ionic radius of K^+, which can more effectively shield the surface charges [56,57].

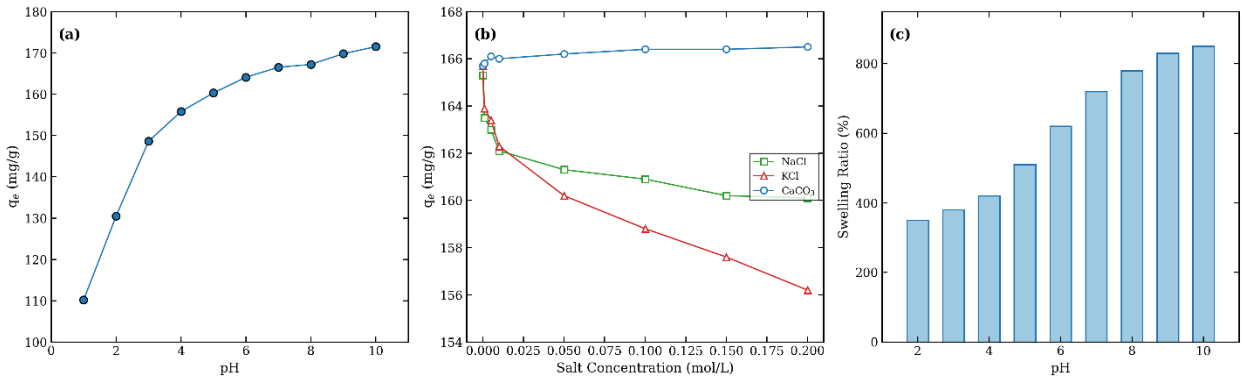

Figure 4. *Combined panel: (a) Effect of solution pH on FB adsorption capacity; (b) Effect of ionic strength (NaCl, KCl, $CaCO_3$) on FB adsorption; (c) Swelling ratio of GO/P(PVP-AAc) at different pH values.*

3.7. Swelling Behavior

The swelling characteristics of the nanocomposite hydrogel play a pivotal role in its adsorption performance, since the degree of swelling controls the diffusion of dye molecules into the three-dimensional polymer network. The equilibrium swelling ratio of the GO/P(PVP-AAc) nanocomposite was found to be pH-dependent. In acidic conditions (pH 2–4), the swelling ratio was relatively low (approximately 350–420%), because the carboxyl groups remain largely protonated and the polymer chains are more compact due to intramolecular hydrogen bonding. As the pH increased toward neutral and basic conditions (pH 7–10), the swelling ratio rose substantially to 750–850%, driven by the ionization of –COOH groups to $–COO^-$, which increases the osmotic pressure within the gel and causes the network to expand [58,59].

This swelling behavior has direct implications for adsorption: at higher pH, the expanded gel network permits greater access of dye molecules to internal binding sites, complementing the electrostatic enhancement described in Section 3.5. The incorporation of GO sheets within the hydrogel matrix provided additional mechanical stability, ensuring that the nanocomposite maintained its structural integrity even at high swelling ratios, which is a critical requirement for practical applications involving repeated use [60].

3.8. Regeneration and Reusability

The ability to regenerate and reuse an adsorbent is crucial for its economic and environmental viability. Five FB dye adsorption–desorption cycles were performed on the GO/P(PVP-AAc) nanocomposite. Figure 5 shows that removal effectiveness declined slightly from 98.2% in the first cycle to 91.7% in the fifth. Due to the irreversible occupation of a tiny fraction of high-energy binding sites and slight structural changes in the hydrogel network during repeated swelling and deswelling, this slow drop occurs [61]. However, over 91% efficiency after five cycles shows the material's durability and practicality. Alkaline regeneration (0.1 mol/L NaOH) broke the electrostatic and hydrogen-bonding connections between adsorbed FB and the surface, releasing dye into solution. These findings imply that the GO/P(PVP-AAc) nanocomposite could be a cost-effective, reusable wastewater treatment adsorbent [62,63].

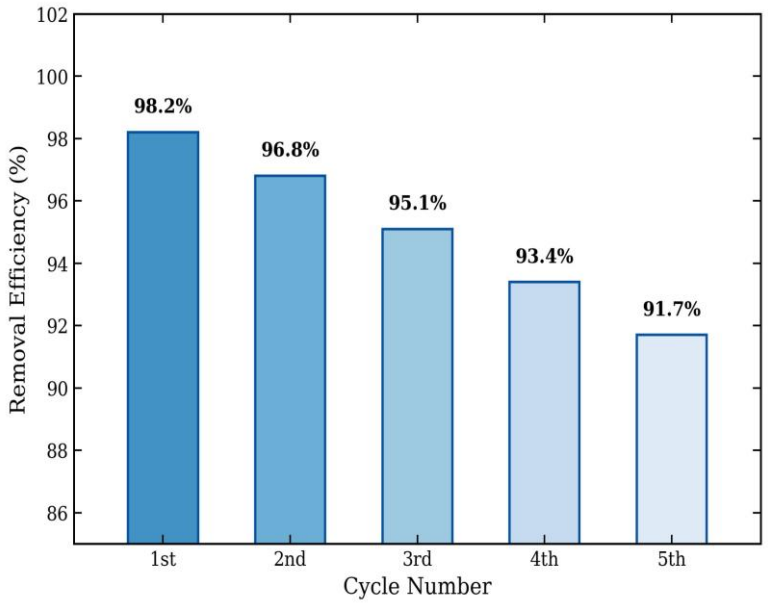

Figure 5. *Regeneration and reusability of GO/P(PVP-AAc) nanocomposite over five adsorption–desorption cycles for FB dye removal.*

3.9. Comparison with Other Adsorbents

Table 4. Comparison of the FB adsorption capacity of GO/P(PVP-AAc) with reported adsorbents.

Adsorbent	q_m (mg/g)	Kinetic Model	Ref.
Activated carbon from rice husk	72.5	PSO	[64]
Montmorillonite clay	89.3	PSO	[65]
Chitosan/GO composite	142.7	PSO	[66]
Fe_3O_4/SiO_2 nanoparticles	98.1	PSO	[67]
GO/P(PVP-AAc) nanocomposite (this work)	**192.31**	PSO	Present study

As indicated in Table 4, the GO/P(PVP-AAc) nanocomposite synthesized in the present study exhibits a higher maximum adsorption capacity for FB compared to several other adsorbents reported in the literature. This superior performance can be attributed to the synergistic combination of the high surface area and functional group density of GO with the swellable, porous three-dimensional polymer network of PVP/AAc, which together provide a large number of accessible and diverse binding sites for the cationic dye molecules.

4. CONCLUSION

In this study, a graphene oxide/polyvinylpyrrolidone/acrylic acid (GO/P(PVP-AAc)) nanocomposite hydrogel was successfully prepared and systematically evaluated as an adsorbent for the removal of Fuchsin Basic dye from aqueous solutions. FTIR, XRD, and FESEM investigations confirmed GO nanosheet absorption into the hydrogel matrix and showed a porous, amorphous structure for adsorption. The equilibrium FB adsorption duration was 120 min. Kinetic study shows chemisorption as the primary rate-controlling mechanism, with a pseudo-second-order model (R^2 = 0.9985). The Freundlich equation fit equilibrium data best of the three isotherm models, indicating heterogeneous, multilayer adsorption on a non-uniform surface. Thermodynamic evaluation showed that FB adsorption onto the nanocomposite

is spontaneous ($\Delta G° < 0$) and exothermic ($\Delta H° = -7.89$ kJ/mol), with a decrease in entropy ($\Delta S° < 0$) reflecting increased ordering at the interface. Due to the electrostatic interaction between the cationic dye and the deprotonated anionic surface, solution pH greatly affected adsorption capacity, with the greatest absorption under alkaline circumstances. Ionic strength studies show that NaCl and KCl decrease adsorption through competition, while $CaCO_3$ marginally increases it through salting-out. Excellent swelling behaviour, especially at increasing pH, allowed dye diffusion into the gel interior of the nanocomposite. After five regeneration cycles, the adsorbent preserved over 91% removal effectiveness, indicating its potential for recurring wastewater treatment. These findings collectively establish the GO/P(PVP-AAc) nanocomposite hydrogel as a highly efficient, reusable, and economically viable material for the remediation of FB-contaminated water.

Conflict of interest: NIL
Funding: NIL

REFERENCES

[1] M.T. Yagub, T.K. Sen, S. Afroze, H.M. Ang, Dye and its removal from aqueous solution by adsorption: A review, Adv. Colloid Interface Sci. 209 (2014) 172–184.

[2] A. Tkaczyk, K. Mitrowska, A. Posyniak, Synthetic organic dyes as contaminants of the aquatic environment and their implications for ecosystems: A review, Sci. Total Environ. 717 (2020) 137222.

[3] V.K. Gupta, Suhas, Application of low-cost adsorbents for dye removal – A review, J. Environ. Manage. 90 (2009) 2313–2342.

[4] R. Jain, M. Mathur, S. Sikarwar, A. Mittal, Removal of the hazardous dye rhodamine B through photocatalytic and adsorption treatments, J. Environ. Manage. 85 (2007) 956–964.

[5] G. Crini, Non-conventional low-cost adsorbents for dye removal: A review, Bioresour. Technol. 97 (2006) 1061–1085.

[6] V. Katheresan, J. Kansedo, S.Y. Lau, Efficiency of various recent wastewater dye removal methods: A review, J. Environ. Chem. Eng. 6 (2018) 4676–4697.

[7] M. Rafatullah, O. Sulaiman, R. Hashim, A. Ahmad, Adsorption of methylene blue on low-cost adsorbents: A review, J. Hazard. Mater. 177 (2010) 70–80.

[8] A. Bhatnagar, M. Sillanpää, Utilization of agro-industrial and municipal waste materials as potential adsorbents for water treatment, Chem. Eng. J. 157 (2010) 277–296.

[9] F. Zhao, E. Repo, D. Yin, M.E.T. Sillanpää, Adsorption of Cd(II) and Pb(II) by a novel EGTA-modified chitosan material, J. Colloid Interface Sci. 409 (2013) 174–182.

[10] Z. Aksu, Application of biosorption for the removal of organic pollutants: A review, Process Biochem. 40 (2005) 997–1026.

[11] E.S. Dragan, Design and applications of interpenetrating polymer network hydrogels: A review, Chem. Eng. J. 243 (2014) 572–590.

[12] N. Sahiner, S. Demirci, M. Sahiner, S. Yilmaz, H. Al-Lohedan, The use of superporous p(3-acrylamidopropyl)trimethyl ammonium chloride cryogels for removal of toxic arsenate anions, J. Environ. Manage. 152 (2015) 66–74.

[13] D.R. Dreyer, S. Park, C.W. Bielawski, R.S. Ruoff, The chemistry of graphene oxide, Chem. Soc. Rev. 39 (2010) 228–240.

[14] S. Park, R.S. Ruoff, Chemical methods for the production of graphenes, Nat. Nanotechnol. 4 (2009) 217–224.

[15] H. Bai, C. Li, X. Wang, G. Shi, A pH-sensitive graphene oxide composite hydrogel, Chem. Commun. 46 (2010) 2376–2378.

[16] L. Zhang, Z. Wang, C. Xu, Y. Li, J. Gao, W. Wang, Y. Liu, High strength graphene

oxide/polyvinyl alcohol composite hydrogels, J. Mater. Chem. 21 (2011) 10399–10406.

[17] N.A. Peppas, J.Z. Hilt, A. Khademhosseini, R. Langer, Hydrogels in biology and medicine: From molecular principles to bionanotechnology, Adv. Mater. 18 (2006) 1345–1360.

[18] L. Fan, C. Luo, M. Sun, H. Qiu, X. Li, Synthesis of magnetic β-cyclodextrin-chitosan/graphene oxide as nanoadsorbent, Colloids Surf. B 95 (2012) 42–49.

[19] T.S. Anirudhan, S.R. Rejeena, Adsorption/desorption of phosphate functionalized nanocellulose, J. Colloid Interface Sci. 381 (2012) 125–136.

[20] W.S. Hummers, R.E. Offeman, Preparation of graphitic oxide, J. Am. Chem. Soc. 80 (1958) 1339.

[21] D.C. Marcano, D.V. Kosynkin, J.M. Berlin, A. Sinitskii, Z. Sun, A. Slesarev, L.B. Alemany, W. Lu, J.M. Tour, Improved synthesis of graphene oxide, ACS Nano 4 (2010) 4806–4814.

[22] S.K. Bajpai, S. Johnson, Superabsorbent hydrogels for removal of divalent toxic ions, React. Funct. Polym. 62 (2005) 271–283.

[23] J. Zhang, Q. Wang, A. Wang, Synthesis and characterization of chitosan-g-poly(acrylic acid)/attapulgite superabsorbent composites, Carbohydr. Polym. 68 (2007) 367–374.

[24] A.K. Sarma, P. Konwarh, R. Bora, Characterization techniques in nanotechnology, in: Nanomaterials Synthesis, Elsevier, 2019, pp. 83–120.

[25] Y.S. Ho, G. McKay, Pseudo-second order model for sorption processes, Process Biochem. 34 (1999) 451–465.

[26] S. Chatterjee, M.W. Lee, S.H. Woo, Adsorption of Congo red by chitosan hydrogel beads impregnated with carbon nanotubes, Bioresour. Technol. 101 (2010) 1800–1806.

[27] S. Lagergren, Zur Theorie der sogenannten Adsorption gelöster Stoffe, K. Sven. Vetenskapsakad. Handl. 24 (1898) 1–39.

[28] I. Langmuir, The adsorption of gases on plane surfaces of glass, mica, and platinum, J. Am. Chem. Soc. 40 (1918) 1361–1403.

[29] H.M.F. Freundlich, Over the adsorption in solution, J. Phys. Chem. 57 (1906) 385–471.

[30] Y. Liu, Is the free energy change of adsorption correctly calculated?, J. Chem. Eng. Data 54 (2009) 1981–1985.

[31] J. Li, A. Mooney, Designing hydrogels for controlled drug delivery, Nat. Rev. Mater. 1 (2016) 16071.

[32] M. Naushad, T. Ahamad, G. Sharma, A.H. Al-Muhtaseb, A.B. Albadarin, M.M. Alam, Z.A. ALOthman, S.M. Alshehri, A.A. Ghfar, Synthesis and characterization of a new starch/SnO_2 nanocomposite for efficient adsorption of toxic Hg^{2+} metal ion, Chem. Eng. J. 300 (2016) 306–316.

[33] J. Chen, B. Yao, C. Li, G. Shi, An improved Hummers method for eco-friendly synthesis of graphene oxide, Carbon 64 (2013) 225–229.

[34] S. Stankovich, D.A. Dikin, R.D. Piner, K.A. Kohlhaas, A. Kleinhammes, Y. Jia, Y. Wu, S.T. Nguyen, R.S. Ruoff, Synthesis of graphene-based nanosheets via chemical reduction of exfoliated graphite oxide, Carbon 45 (2007) 1558–1565.

[35] M.A. Ahmad, R. Alrozi, Removal of malachite green dye from aqueous solution using rambutan peel-based activated carbon, Chem. Eng. J. 171 (2011) 510–516.

[36] A.K. Mishra, S. Ramaprabhu, Functionalized graphene sheets for arsenic removal and desalination of seawater, Desalination 282 (2011) 39–45.

[37] Y. Li, Q. Du, T. Liu, X. Peng, J. Wang, J. Sun, Y. Wang, S. Wu, Z. Wang, Y. Xia, L. Xia, Comparative study of methylene blue dye

adsorption onto activated carbon, graphene oxide, and carbon nanotubes, Chem. Eng. Res. Des. 91 (2013) 361–368.

[38] S.H. Huo, X.P. Yan, Facile magnetization of metal-organic framework MIL-101 for magnetic solid-phase extraction of polycyclic aromatic hydrocarbons in environmental water samples, Analyst 137 (2012) 3445–3451.

[39] Y.S. Ho, G. McKay, Sorption of dye from aqueous solution by peat, Chem. Eng. J. 70 (1998) 115–124.

[40] Y.S. Ho, Citation review of Lagergren kinetic rate equation on adsorption reactions, Scientometrics 59 (2004) 171–177.

[41] W.J. Weber, J.C. Morris, Kinetics of adsorption on carbon from solution, J. Sanit. Eng. Div. 89 (1963) 31–60.

[42] L. Liu, C. Li, C. Bao, Q. Jia, P. Xiao, X. Liu, Q. Zhang, Preparation and characterization of chitosan/graphene oxide composites for the adsorption of Au(III) and Pd(II), Talanta 93 (2012) 350–357.

[43] G. Sharma, M. Naushad, D. Pathania, A. Mittal, G.E. El-Desoky, Modification of Hibiscus cannabinus fiber by graft copolymerization: Application for dye removal, Desalin. Water Treat. 54 (2015) 3114–3121.

[44] C.H. Giles, T.H. MacEwan, S.N. Nakhwa, D. Smith, Studies in adsorption. Part XI. A system of classification of solution adsorption isotherms, J. Chem. Soc. (1960) 3973–3993.

[45] K.R. Hall, L.C. Eagleton, A. Acrivos, T. Vermeulen, Pore- and solid-diffusion kinetics in fixed-bed adsorption under constant-pattern conditions, Ind. Eng. Chem. Fundam. 5 (1966) 212–223.

[46] M.I. Temkin, V. Pyzhev, Kinetics of ammonia synthesis on promoted iron catalysts, Acta Physicochim. URSS 12 (1940) 217–222.

[47] A.S. Özcan, B. Erdem, A. Özcan, Adsorption of Acid Blue 193 from aqueous solutions onto Na-bentonite and DTMA-bentonite, J. Colloid Interface Sci. 280 (2004) 44–54.

[48] E. Demirbas, M. Kobya, E. Senturk, T. Ozkan, Adsorption kinetics for the removal of chromium (VI) from aqueous solutions on the activated carbons, Water SA 30 (2004) 533–539.

[49] M.J. Jaycock, G.D. Parfitt, Chemistry of Interfaces, Ellis Horwood Ltd., Chichester, 1981.

[50] G. McKay, H.S. Blair, J.R. Gardner, Adsorption of dyes on chitin. I. Equilibrium studies, J. Appl. Polym. Sci. 27 (1982) 3043–3057.

[51] Z. Bekci, Y. Seki, M.K. Yurdakoc, Equilibrium studies for trimethoprim adsorption on montmorillonite KSF, J. Hazard. Mater. 133 (2006) 233–242.

[52] G.E. Boyd, A.W. Adamson, L.S. Myers Jr., The exchange adsorption of ions from aqueous solutions by organic zeolites. II. Kinetics, J. Am. Chem. Soc. 69 (1947) 2836–2848.

[53] G. Annadurai, R.S. Juang, D.J. Lee, Use of cellulose-based wastes for adsorption of dyes from aqueous solutions, J. Hazard. Mater. 92 (2002) 263–274.

[54] B.H. Hameed, D.K. Mahmoud, A.L. Ahmad, Equilibrium modeling and kinetic studies on the adsorption of basic dye by a low-cost adsorbent: Coconut (Cocos nucifera) bunch waste, J. Hazard. Mater. 158 (2008) 65–72.

[55] A.T. Paulino, M.R. Guilherme, A.V. Reis, G.M. Campese, E.C. Muniz, J. Nozaki, Removal of methylene blue dye from an aqueous media using superabsorbent hydrogel supported on modified polysaccharide, J. Colloid Interface Sci. 301 (2006) 55–62.

[56] G. Crini, P.M. Badot, Application of chitosan, a natural aminopolysaccharide, for dye removal from aqueous solutions by adsorption processes, Prog. Polym. Sci. 33 (2008) 399–447.

[57] W.T. Tsai, C.Y. Chang, C.H. Ing, C.F. Chang, Adsorption of acid dyes from aqueous solution on activated bleaching earth, J. Colloid Interface Sci. 275 (2004) 72–78.

[58] L. Brannon-Peppas, N.A. Peppas, Equilibrium swelling behavior of pH-sensitive hydrogels, Chem. Eng. Sci. 46 (1991) 715–722.

[59] T.R. Hoare, D.S. Kohane, Hydrogels in drug delivery: Progress and challenges, Polymer 49 (2008) 1993–2007.

[60] R. Liu, S. Liang, X.Z. Tang, D. Yan, X. Li, Z.Z. Yu, Tough and highly stretchable graphene oxide/polyacrylamide nanocomposite hydrogels, J. Mater. Chem. 22 (2012) 14160–14167.

[61] S.T. Akar, A.S. Ozcan, T. Akar, A. Ozcan, Z. Kaynak, Biosorption of a reactive textile dye from aqueous solutions utilizing an agro-waste, Desalination 249 (2009) 757–761.

[62] G. Sharma, M. Naushad, A. Kumar, S. Rana, S. Sharma, A. Bhatnagar, F.J. Stadler, A.A. Ghfar, M.R. Khan, Efficient removal of coomassie brilliant blue R-250 dye using starch/poly(alginic acid-cl-acrylamide) nanohydrogel, Process Saf. Environ. Prot. 109 (2017) 301–310.

[63] X. Li, H. Zhou, W. Wu, S. Wei, Y. Xu, Y. Kuang, Studies of heavy metal ion adsorption on Chitosan/Sulfydryl-functionalized graphene oxide composites, J. Colloid Interface Sci. 448 (2015) 389–397.

[64] R.L. Tseng, F.C. Wu, R.S. Juang, Liquid-phase adsorption of dyes and phenols using pinewood-based activated carbons, Carbon 41 (2003) 487–495.

[65] P. Baskaralingam, M. Pulikesi, D. Elango, V. Ramamurthi, S. Sivanesan, Adsorption of acid dye onto organobentonite, J. Hazard. Mater. 128 (2006) 138–144.

[66] L. Fan, C. Luo, M. Sun, X. Li, H. Qiu, Highly selective adsorption of lead ions by water-dispersible magnetic chitosan/graphene oxide composites, Colloids Surf. B 103 (2013) 523–529.

[67] L. Zhang, H. Li, Y. Liu, Z. Tian, B. Yang, Z. Sun, S. Yan, Adsorption-reduction removal of Cr(VI) by tobacco petiole pyrolytic biochar, Bioresour. Technol. 268 (2018) 149–157.